Linear and nonlinear instabilities in rotating cylindrical Rayleigh-Bénard convection

Ligang Li,[1] Xinhao Liao,[1] Kit H. Chan,[2] and Keke Zhang[3]

[1]*Shanghai Astronomical Observatory, Chinese Academy of Sciences, Shanghai 200030, China*
[2]*Department of Mathematics, The University of Hong Kong, Pokfulam, Hong Kong*
[3]*Department of Mathematical Sciences, University of Exeter, EX4 4QE, United Kingdom*

Linear and nonlinear convection in a rotating annular cylinder, under experimental boundary conditions, heated from below and rotating about a vertical axis are investigated. In addition to the usual physical parameters such as the Rayleigh and Taylor number, an important geometric parameter, the ratio of the inner to outer radius, enters into the problem. For intermediate ratios, linear stability analysis reveals that there exist two countertraveling convective waves which are nonlinearly significant: a retrograde wave located near the outer sidewall and a prograde wave adjacent to the inner sidewall. Several interesting phenomena of nonlinear convection are found: (i) tempospatially modulated countertraveling waves caused by an instability of the Eckhaus-Benjamin-Feir type, (ii) destructive countertraveling waves in which the existence or disappearance of the prograde wave is determined by its relative phase to the retrograde wave, and (iii) a saddle-node-type bifurcation in which the prograde wave takes an infinite amount of time to pass over the retrograde wave.

I. INTRODUCTION

Rotating convection in cylindrical geometry is often employed to illustrate and understand the fundamental dynamics taking place in planetary fluid interiors and atmospheres (see, for example, Refs. [1–7]). As a consequence of the influence of rotation and of the sidewall, linear convective instabilities in rotating cylindrical Rayleigh-Bénard systems uniformly heated from below are always in the form of azimuthally traveling waves (e.g., Refs. [8,9,2,10]). Theoretical generic properties of linear instabilities and nonlinear bifurcations in rotating cylindrical convection were discussed by [11] (see also Ref. [12]). The present study is primarily concerned with linear and nonlinear convection in a rotating annular cylinder, under experimental boundary conditions, heated from below and rotating about a vertical axis, which is experimentally realizable. In comparison to the classical Rayleigh-Bénard convection, the ratio of the inner (r_i) to outer (r_o) radius enters into the problem as a geometric parameter which plays an essential role in the dynamics of nonlinear convection.

It is well known that, in rotating cylindrical systems near the threshold of linear convective instabilities, a spatially periodic traveling wave dominated by a single wave number m is usually selected by nonlinearity (see, for example, Ref. [11]). An interesting physical phenomenon in rotating convection is the existence of multiple traveling waves. Suppose that there exist two linear countertraveling wave solutions at the onset of convective instabilities in a rotating annular cylinder given by

$$\mathbf{u} = \mathbf{u}_p(s,z)e^{i(m_p\phi-\omega_p t)} + \mathbf{u}_r(s,z)e^{i(m_r\phi+\omega_r t)}, \qquad (1)$$

where $\mathbf{u}$ represents the fluid velocity, m denotes the azimuthal wave number, and ω is the frequency: the subscripts p and r denote a progradely traveling wave and a retrogradely traveling wave, respectively. Here (s,ϕ,z) are cylindrical coordinates with $s=0$ at the axis of rotation. It is anticipated that nonlinear competition between the two waves

just beyond threshold can yield three possible equilibria: a progradely traveling wave or a retrogradely traveling wave, or a standing wave if $\mathbf{u}_p=\mathbf{u}_r$, $m_p=m_r$, and $\omega_p=\omega_r$. A major question is the nature of further nonlinear instabilities away from threshold as well as the new equilibrium states led by the instabilities. For a nonlinear traveling wave, a well-known instability is of the Eckhaus-Benjamin-Feir type in which the wave becomes unstable by resonant excitation of the neighboring waves leading to spatial and temporal modulation. However, if two countertraveling waves are spatially located in different places, as in the case of the present problem, nonlinear competition and interaction between the two countertraveling waves can be quite different. It is worth noting that the phenomenon of multiple traveling waves with different spatial locations in rotating convective systems is perhaps responsible for multiple zonal patterns observed in giant planets (e.g., Ref. [13]).

The physical and mathematical properties of nonlinear multiple traveling waves with different locations are not well understood. For rotating annular cylinders with moderate radius ratios in which the problem of linear convection is characterized by two countertraveling waves located in different regions, we know very little about the nonlinear properties of the waves. When the radius ratio is small, the nonlinear interaction between the two countertraveling waves is weak and, consequently, the two waves can be treated separately (e.g., Refs. [14–16]). In Ref. [17], it was found that weakly nonlinear interaction at the radius ratio $r_i/r_o=0.625$ can lead to weakly irregular nonlinear convection at relatively small Rayleigh numbers. In this study, we extend the previous work by performing a systematic analysis of linear convective instabilities over a wide range of the ratio r_i/r_o and by carrying out many nonlinear simulations over a wide range of the Rayleigh number Ra for a larger radius ratio $r_i/r_o=0.75$, at which strongly nonlinear interaction between the two countertraveling waves can occur. In particular, we unveil three interesting phenomena of nonlinear convection in a rotating annular cylinder under experimental boundary conditions with Prandtl number Pr=7.0 (water at room tempera-
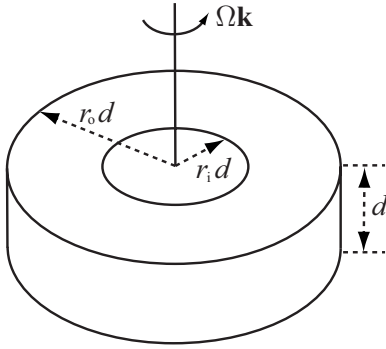
FIG. 1. Geometry of a rotating annular cylinder of depth d with cross section defined by $(r_i d) \leq s \leq (r_o d)$, s being the distance from the rotation axis.

ture): (a) tempospatially modulated countertraveling waves in connection with an instability of the Eckhaus-Benjamin-Feir type, (b) destructive countertraveling waves in which the existence of the prograde wave is determined by its phase relative to the retrograde wave, and (c) a saddle-node-type bifurcation in which the prograde wave takes an infinitely long time to move away from the retrograde wave.

The rotating cylindrical convection studied in this paper does not share all the well-known behavior exhibited in an infinitely extended Rayleigh-Bénard layer. This is because convective wave motions in rotating cylindrical systems are not only geometrically restricted by the existence of curved sidewalls, but also dynamically restrained by the effect of rotation, through the curved sidewalls, which forces the fluid motions to be spatially localized and radially asymmetric (e.g., Refs. [8,2,18]). It is both the geometric and dynamic constraints that produce a unique and intriguing nonlinear phenomenon involving the two countertraveling waves, which will be discussed in the present study. Moreover, it should be noted that, for a moderate ratio such as r_i/r_o =0.75, the curvature effect is physically significant and, consequently, the coupled complex Ginzburg-Landau equations based on expansion in the small amplitude of convection are, generally speaking, no longer applicable. The main reason is that the two oppositely traveling modes are characterized not only by different frequencies and wave numbers, but also by different critical Rayleigh numbers. It follows that the approach of a direct three-dimensional numerical simulation over a wide range of the Rayleigh number, which is computationally demanding and expensive, has to be employed in order to elucidate various nonlinear bifurcations away from threshold.

In what follows we shall begin by presenting the mathematical equations of the problem in Sec. II. Linear stability analysis is presented in Sec. III while the numerical method and the results of nonlinear convection are discussed in Sec. IV with a summary and remarks given in Sec. V.

II. MATHEMATICAL FORMULATION OF THE PROBLEM

We consider convection in a Boussinesq fluid with constant thermal diffusivity κ, thermal expansion coefficient α, and kinematic viscosity ν confined in an annular cylinder of

depth d with inner radius $r_i d$ and outer radius $r_o d$, the geometry of which is shown in Fig. 1. The vertical coordinate, denoted by z, is parallel to the rotation axis, with radial coordinate s and azimuthal coordinate ϕ. The whole system rotates uniformly with constant angular velocity $\Omega \hat{\mathbf{z}}$ in the presence of constant vertical gravity

$$\mathbf{g} = -g_0 \hat{\mathbf{z}}, \tag{2}$$

where $\hat{\mathbf{z}}$ (or $\mathbf{k}$) is a vertical unit vector. As in the classical Rayleigh-Bénard problem, the annular cylinder is uniformly heated from below to maintain an unstable vertical temperature gradient

$$\nabla \Theta_0 = -\beta \hat{\mathbf{z}}, \tag{3}$$

where β is a positive constant. Convective instabilities take place when β is sufficiently large. The convection problem is governed by the three dimensionless equations

$$\frac{\partial \mathbf{u}}{\partial t} + \mathbf{u} \cdot \nabla \mathbf{u} + \mathrm{Ta}^{1/2} \hat{\mathbf{z}} \times \mathbf{u} = -\nabla p + \mathrm{Ra}\Theta \mathbf{k} + \nabla^2 \mathbf{u}, \tag{4}$$

$$\mathrm{Pr}\left(\frac{\partial \Theta}{\partial t} + \mathbf{u} \cdot \nabla \Theta \right) = \mathbf{u} \cdot \hat{\mathbf{z}} + \nabla^2 \Theta, \tag{5}$$

$$\nabla \cdot \mathbf{u} = 0, \tag{6}$$

where Θ represents the dimensionless deviation of the temperature from its conducting state Θ_0, p is the total pressure and $\mathbf{u}$ is the three-dimensional velocity field $\mathbf{u} = (u_s, u_\phi, u_z)$ in the cylindrical coordinates (s, ϕ, z) with corresponding unit vectors $(\hat{\mathbf{s}}, \hat{\boldsymbol{\phi}}, \hat{\mathbf{z}})$. The problem is characterized by three nondimensional parameters, the Rayleigh number Ra, the Prandtl number Pr, and the Taylor number Ta:

$$\mathrm{Ra} = \frac{\alpha \beta g_0 d^4}{\nu \kappa}, \quad \mathrm{Pr} = \frac{\nu}{\kappa}, \quad \mathrm{Ta} = \frac{4\Omega^2 d^4}{\nu^2}.$$

Additionally, there is an important geometric parameter, χ, defined as the ratio of the inner to outer radius, i.e., $\chi = r_i/r_o$. The boundary conditions are assumed to be no-slip and conducting at the top and bottom

$$u_s = u_\phi = u_z = \Theta = 0 \quad \text{at } z = 0, 1, \tag{7}$$

while the no-slip and insulating sidewalls require that

$$u_s = u_\phi = u_z = \frac{\partial \Theta}{\partial s} = 0 \quad \text{at } s = r_i, \quad r_o. \tag{8}$$

We shall first undertake the stability analysis of linearized versions of Eqs. (4)–(6) subject to the boundary conditions (7) and (8). Our emphasis will be placed on illustrating the characteristics of progradely and retrogradely traveling waves at the onset of convection. We then solve the fully nonlinear equations (4)–(6) subject to the same boundary conditions by direct three-dimensional numerical simulations as an initial-value problem, attempting to identify different nonlinear states resulting from various nonlinear instabilities.

III. LINEAR STABILITY ANALYSIS

A. Numerical method

In rotating cylindrical systems, it is anticipated that the most unstable mode of convective instabilities is nonaxisymmetric (e.g., Refs. [8,14]). For the purpose of numerical analysis, a nonaxisymmetric velocity vector satisfying Eq. (6) in cylindrical geometry can be expressed in terms of two scalar potentials Ψ and Φ [19]

$$\mathbf{u} = \frac{1}{s}\frac{\partial\Psi}{\partial\phi}\hat{\mathbf{s}} + \left(\frac{\partial\Phi}{\partial z} - \frac{\partial\Psi}{\partial s}\right)\hat{\boldsymbol{\phi}} - \frac{1}{s}\frac{\partial\Phi}{\partial\phi}\hat{\mathbf{z}}. \qquad (9)$$

In terms of Ψ and Φ, the non-slip velocity conditions on the sidewall and on the top and bottom are imposed by

$$\Psi = \frac{\partial\Psi}{\partial s} = \Phi = 0 \quad \text{at } s = r_i, \quad r_o \qquad (10)$$

and

$$\Psi = \frac{\partial\Phi}{\partial z} = \Phi = 0 \quad \text{at } z = 0, 1. \qquad (11)$$

Making use of the expression (9) and applying $\hat{\mathbf{z}}\cdot\nabla\times$ and $\hat{\mathbf{s}}\cdot\nabla\times$ onto the linearized Eq. (4), we can derive the three independent scalar equations

$$0 = \left(\frac{\partial}{\partial t} - \nabla^2\right)\left[\frac{1}{s}\frac{\partial}{\partial s}\left(s\frac{\partial\Phi}{\partial z}\right) - \left(\nabla^2 - \frac{\partial^2}{\partial z^2}\right)\Psi\right] + \frac{\text{Ta}^{1/2}}{s}\frac{\partial^2\Phi}{\partial z\partial\phi}, \qquad (12)$$

$$\begin{aligned}0 = &-\frac{\text{Ra}}{s}\frac{\partial\Theta}{\partial\phi} + \left[\frac{\partial}{\partial t} - \left(\nabla^2 + \frac{2}{s}\frac{\partial}{\partial s} + \frac{1}{s^2}\right)\right] \\ &\times\left[\frac{\partial^2\Psi}{\partial s\partial z} - \left(\nabla^2 - \frac{1}{s}\frac{\partial}{\partial s}s\frac{\partial}{\partial s}\right)\Phi\right] - \frac{\text{Ta}^{1/2}}{s}\frac{\partial^2\Psi}{\partial z\partial\phi} \\ &- \frac{1}{s}\left[\frac{1}{s}\frac{\partial}{\partial s}\left(s\frac{\partial^2\Phi}{\partial z^2}\right) - \left(\nabla^2 - \frac{\partial^2}{\partial z^2}\right)\frac{\partial\Psi}{\partial z}\right], \qquad (13)\end{aligned}$$

$$0 = \left[\nabla^2 - \text{Pr}\frac{\partial}{\partial t}\right]\Theta - \frac{1}{s}\frac{\partial\Phi}{\partial\phi}. \qquad (14)$$

The linear problem, governed by the three partial differential equations (12)–(14), is then solved numerically by using the Chebyshev-tau method. For an azimuthally traveling linear wave, we can express solutions in the form

$$[\Psi,\Phi,\Theta](s,\phi,z,t) = [\Psi,\Phi,\Theta](s,z)e^{i(m\phi+\omega t)},$$

in which the potential fields $\Phi(s,z)$ and $\Psi(s,z)$, and the temperature deviation $\Theta(s,z)$ are further expanded in terms of the standard Chebyshev functions $T_k(x)$

$$\Psi = (1-\tilde{s}^2)^2(1-\tilde{z}^2)\sum_{j=0}^{J}\sum_{l=0}^{L}\Psi_{jl}T_j(\tilde{s})T_l(\tilde{z}), \qquad (15)$$

$$\Phi = (1-\tilde{s}^2)(1-\tilde{z}^2)^2\sum_{j=0}^{J}\sum_{l=0}^{L}\Phi_{jl}T_j(\tilde{s})T_l(\hat{z}), \qquad (16)$$
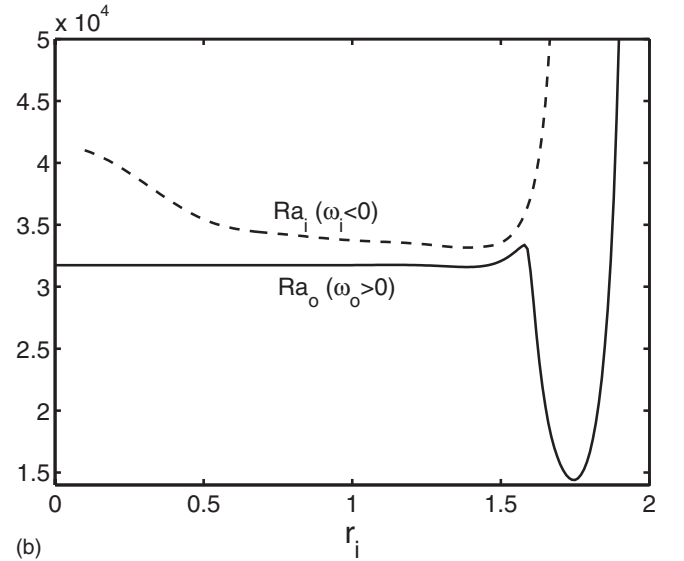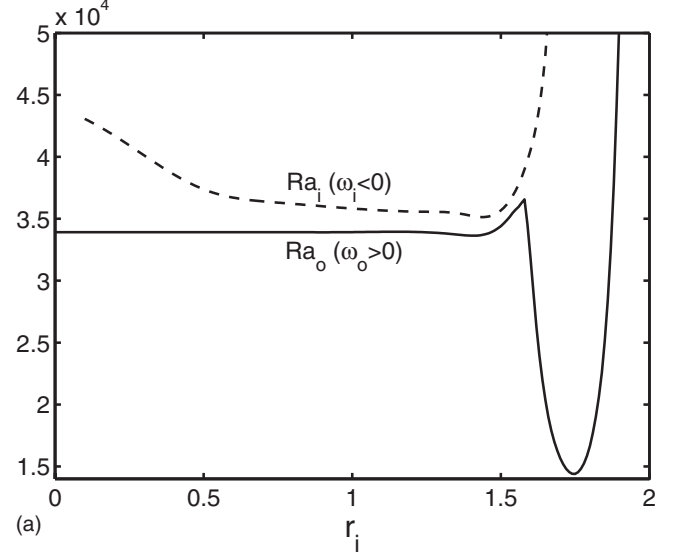
FIG. 2. The Rayleigh number at the onset of convective instabilities as a function of the inner radius r_i with a fixed $r_o = 2.0$: Ra_o (solid line) represents the Rayleigh number required to excite the retrogradely propagating wave ($\omega_o > 0$) while Ra_i (dashed line) is for the progradely propagating wave ($\omega_i < 0$). In all linear solutions, the Taylor number is fixed to be $\text{Ta} = 10^6$ with (a) for $\text{Pr} = 7.0$ and (b) for $\text{Pr} = 0.7$.

$$\Theta = (1-\tilde{z}^2)\sum_{j=0}^{J+2}\sum_{l=0}^{L}\Theta_{jl}T_j(\tilde{s})T_l(\tilde{z}), \qquad (17)$$

where $\tilde{z} = 2z - 1$ and $\tilde{s} = 2(s-r_i)/(r_o-r_i)-1$, Ψ_{jl}, Φ_{jl}, and Θ_{jl} are complex coefficients which are to be obtained, along with the marginal Rayleigh number Ra and the corresponding azimuthal wave number m and the frequency ω, by a standard numerical procedure. In the expansion for temperature Θ, the two extra terms in Eq. (17) [i.e., $(J+2)$] are needed to enforce the two sidewall boundary conditions for the temperature. With $L = J = O(100)$, our numerical solutions achieve an accuracy within 1%.
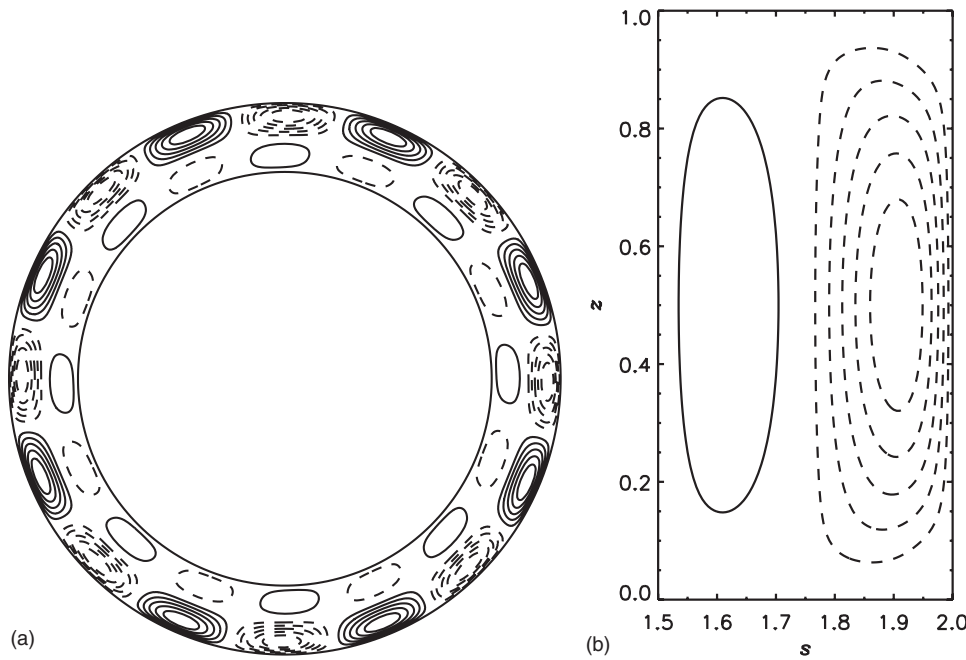
FIG. 3. Contours of u_z (a) in the middle plane $z = 1/2$ and (b) in a vertical plane for the retrograde mode concentrating near the outer sidewall with $Ra_o = 34406$, $m_o = 8$, and $\omega_o = 4.104$ for $\chi = 0.75$, Ta $= 10^6$, and Pr $= 7.0$.

B. Convective instabilities: Retrogradely or progradely propagating waves

The problem of linear stability analysis defined by partial differential equations (12)–(14) subject to experimental boundary conditions (10) and (11), is numerically cumbersome and complicated, but it can not only offer a helpful numerical guidance for nonlinear simulations but also provide valuable physical insights into understanding nonlinear phenomenon. The stability analysis reveals that there exist two different traveling wave solutions at the onset of convective instabilities. The first solution represents a retrogradely propagating wave localized near the outer sidewall defined by

$$\mathbf{u}_o = \mathbf{u}_o(s, z, Ra_o)\exp\{im_o\phi + i\omega_o t\}, \tag{18}$$

in which the Rayleigh number Ra_o is chosen such that ω_o is positive and real for a given wave number $m_o > 0$. The second is a progradely propagating wave located in the vicinity of the inner sidewall defined by

$$\mathbf{u}_i = \mathbf{u}_i(s, z, Ra_i)\exp\{im_i\phi + i\omega_i t\}, \tag{19}$$

where the Rayleigh number Ra_i is chosen such that ω_i is negative and real for a given wave number $m_i > 0$.

In the linear analysis, we fix $r_o = 2.0$ but change r_i such that the radius ratio $\chi = r_i/r_o$ varies between $0 < \chi < 1$. When $\chi \ll 1$, it is known that the effect of the sidewall destabilizes convection and leads to a single retrogradely traveling wave localized near the outer sidewall of the cylinder (e.g., Refs. [8,2,10]). However, it is only at an intermediate ratio that convection can exhibit much richer dynamics and unusual nonlinear bifurcations. This is because the linear problem for intermediate χ is characterized by two different traveling waves: a retrograde mode near the outer sidewall (the outer retrograde mode) and a prograde mode adjacent to the inner sidewall (the inner prograde mode) that has a different wave number, frequency, and critical Rayleigh number. Without

loss of general physics, we shall concentrate on the cases Pr $= 7.0$ (water at room temperature) and Pr $= 0.7$ (air at room temperature) at the fixed outer radius $r_o = 2$ and Taylor number Ta $= 10^6$ for which the convective motion is strongly affected by the effect of rotation.

The linear results are summarized in Fig. 2, suggesting there are no significant differences between the Pr $= 7$ and Pr $= 0.7$ solutions. When the radius ratio χ is small, because of the stronger curvature effect in connection with a small inner cylinder, progradely traveling modes near the inner sidewall require a much larger Rayleigh number to excite and are hence physically and nonlinearly unimportant. As χ increases to about 0.75, however, the difference between Ra_o and Ra_i approximately reaches a minimum and, consequently, both of the countertraveling modes become physically significant. For $\chi = 0.75$ and Pr $= 7.0$ at Ta $= 10^6$, the outer retrograde mode is described by the Rayleigh number $Ra_o = 34406$ with $m_o = 8$ and $\omega_o = 4.104$, while the inner prograde mode is characterized by $Ra_i = 35667$ with $m_i = 7$ and $\omega_i = -4.053$. The profile of the retrograde mode is depicted in Fig. 3, showing the convective motion mainly concentrates in the outer sidewall region. In contrast, the prograde mode is mainly located near the inner sidewall, which is shown Fig. 4. Our linear stability analysis suggests that $Ra_i > Ra_o$ and $m_o > m_i$ for moderate values of χ and for sufficiently large values of Ta. It should be also noted that there exist several different retrograde modes that require slightly larger Rayleigh numbers to excite. For instance, the outer retrograde mode with $m_o = 9$ is characterized by the Rayleigh number $Ra_o = 34\,498$ with $\omega_o = 3.957$, suggesting possible multiple nonlinear equilibria near threshold.

IV. NONLINEAR CONVECTIVE FLOWS

A. Numerical method

We tackle the problem of nonlinear convection via direct three-dimensional numerical simulations using a finite differ-
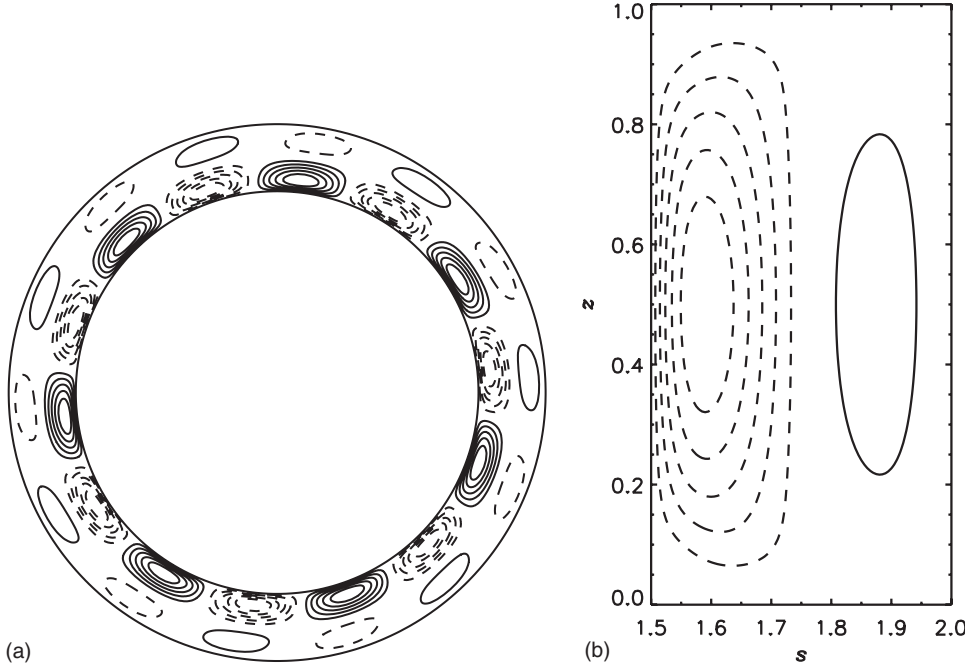
FIG. 4. Contours of u_z (a) in the middle plane $z=1/2$ and (b) in a vertical plane for the prograde mode concentrating near the inner sidewall with $Ra_i=35667$ with $m_i=7$, $\omega_i=-4.053$ for $\chi=0.75$, $Ta=10^6$, and $Pr=7.0$.

ence method. A second-order finite difference scheme with staggered grids [20] is employed for the spatial discretization of an annular cylinder. We use the integer subscripts (j,i,k) to denote the grid point position (s_j,ϕ_i,z_k) while the subscripts $(j-1/2,i-1/2,k-1/2)$ are used for the midpoint position $(s_{j-1/2},\phi_{i-1/2},z_{k-1/2})$. A sketch of several grid points in cylindrical coordinates is presented in Fig. 5.

A second-order factorization method [21], combined with a Crank-Nicolson scheme, is implemented for the time advancement of numerical integration. In the temporal discretization, the velocity and temperature are decoupled from the pressure through a predictor-corrector procedure as follows. The prediction involves obtaining a temporary velocity $\tilde{\mathbf{u}}$ and the temperature Θ^{n+1} at time t_{n+1} from the two previous values at t_n and t_{n-1}:

$$\left(I - \frac{\Delta t}{2}\mathcal{L}_1\right)\tilde{\mathbf{u}} = \frac{\Delta t}{2}\hat{\mathbf{z}}\mathcal{Q}_1\Theta^{n+1} + \left(I + \frac{\Delta t}{2}\mathcal{L}_1\right)\hat{\mathbf{u}} + \frac{\Delta t}{2}\hat{\mathbf{z}}\mathcal{Q}_1\Theta^n$$
$$+ \Delta t\mathbf{N}_1^{n+1/2}, \qquad (20)$$

$$\left(I - \frac{\Delta t}{2}\mathcal{L}_2\right)\Theta^{n+1} = \frac{\Delta t}{2}\mathcal{Q}_2\tilde{u}_z + \left(I + \frac{\Delta t}{2}\mathcal{L}_2\right)\Theta^n + \frac{\Delta t}{2}\mathcal{Q}_2\hat{u}_z$$
$$+ \Delta tN_2^{n+1/2}, \qquad (21)$$

with

$$\hat{\mathbf{u}} = \mathbf{u}^n - \frac{\Delta t}{2}\mathcal{G}p^n, \qquad (22)$$

where $\mathcal{G}$ denotes a discrete gradient operator, I is the identity matrix, $\mathcal{L}_1, \mathcal{L}_2, \mathcal{Q}_1, \mathcal{Q}_2$ are discrete linear spatial operators which are defined as

$$\mathcal{L}_1\mathbf{u} = \hat{\mathbf{s}}\left(\nabla^2 u_s - \frac{u_s}{s^2} - \frac{2}{s^2}\frac{\partial u_\phi}{\partial \phi} + Ta^{1/2}u_\phi\right)_{j,i-1/2,k-1/2}$$
$$+ \hat{\phi}\left(\nabla^2 u_\phi - \frac{u_\phi}{s^2} + \frac{2}{s^2}\frac{\partial u_s}{\partial \phi} - Ta^{1/2}u_s\right)_{j-1/2,i,k-1/2}$$
$$+ \hat{\mathbf{z}}(\nabla^2 u_z)_{j-1/2,i-1/2,k}, \qquad (23)$$

$$\mathcal{Q}_1\Theta = \frac{Ra}{2}(\Theta_{j-1/2,i-1/2,k-1/2} + \Theta_{j-1/2,i-1/2,k+1/2}), \qquad (24)$$

$$\mathcal{L}_2\Theta = \frac{1}{Pr}(\nabla^2\Theta)_{j-1/2,i-1/2,k-1/2}, \qquad (25)$$

$$\mathcal{Q}_2 u_z = \frac{1}{2Pr}[(u_z)_{j-1/2,i-1/2,k} + (u_z)_{j+1/2,i+1/2,k-1}]. \qquad (26)$$

Furthermore, $\mathbf{N}_1^{n+1/2}$ and $N_2^{n+1/2}$ represent the discrete vector nonlinear term in the momentum equation and the scalar nonlinear term in the heat equation, respectively. They are approximated by the second-order Adams-Bashforth formula in the time domain

$$\mathbf{N}_1^{n+1/2} = \frac{3}{2}\mathbf{N}_1^n - \frac{1}{2}\mathbf{N}_1^{n-1} + O(\Delta t^2), \qquad (27)$$

$$N_2^{n+1/2} = \frac{3}{2}N_2^n - \frac{1}{2}N_2^{n-1} + O(\Delta t^2). \qquad (28)$$

From Eqs. (27) and (28), it can be seen that two previous values are needed to advance time integration, except at the very beginning when, for example, $N_2^{n+1/2}$ is simply set to be N_2^0.

Four steps are generally required to advance the time integration of nonlinear convection. First, for a given velocity $\mathbf{u}^n$ and pressure p^n at $t=t^n$, we solve Eq. (22) to obtain the
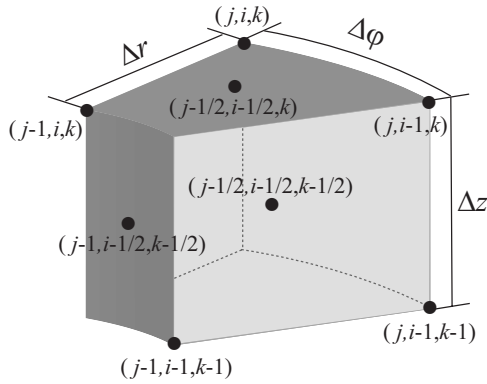
FIG. 5. A sketch of several grid points in cylindrical coordinates.

temporary velocity $\hat{\mathbf{u}}$. Second, $\hat{\mathbf{u}}$ and Θ^n are used to solve Eqs. (20) and (21) to determine $\tilde{\mathbf{u}}$ and Θ^{n+1}. Third, we obtain the pressure p^{n+1} by solving the Poisson equation

$$\frac{\Delta t}{2} \mathcal{DG} p^{n+1} = \mathcal{D}\tilde{\mathbf{u}}, \tag{29}$$

using the temporary velocity $\tilde{\mathbf{u}}$, where $\mathcal{D}$ is a discrete divergence operator. In the final step, the velocity $\mathbf{u}^{n+1}$ is obtained from $\tilde{\mathbf{u}}$ by the correction procedure, using the newly derived pressure p^{n+1}, described by

$$\mathbf{u}^{n+1} = \tilde{\mathbf{u}} - \frac{\Delta t}{2} \mathcal{G} p^{n+1}, \tag{30}$$

so that the incompressible condition is satisfied. The accuracy of our nonlinear simulations was checked by calculating nonlinear solutions at exactly the same parameters but using different spatial and temporal resolutions. Typically, we have used the spatial resolution $[50 \times 400 \times 50]$ in the (s, ϕ, z) directions, respectively, for the nonlinear solutions presented in this paper.

B. Supercritical primary bifurcation

The main objective of our nonlinear study is to identify various nonlinear states in connection with the interaction of two countertraveling waves. This is achieved by carrying out many careful simulations over a wide range of the Rayleigh number Ra while other parameters are fixed. We shall concentrate on the case with $\chi = 0.75$, Ta$= 10^6$, and Pr$= 7.0$.

It should be mentioned that we cannot change control parameters, such as the Taylor number, such that the purely conducting state loses stability simultaneously to both countertraveling modes as Ra increases from a small value. In other words, a codimension-two bifurcation involving two countertraveling modes cannot take place because of the cylindrical curvature effect. Consequently, the nonlinear problem of counter-traveling waves cannot be studied on the basis of the usual two coupled complex Ginzburg-Landau equations.

Our first task is to compute the primary bifurcation from the onset of linear convective instabilities, which not only tests the validity of the linear analysis but also reveals whether the bifurcation is supercritical or subcritical (e.g., Ref. [23]). To measure the nonlinear properties of convection, we introduce the kinetic energy of the flow E_{kin}

$$E_{\mathrm{kin}} = \frac{1}{2} \int_0^1 \int_{r_i}^{r_o} \int_0^{2\pi} |\mathbf{u}|^2 s \, d\phi \, ds \, dz$$

and the Nusselt number Nu for convective heat transport

$$\mathrm{Nu} = 1 - \frac{\mathrm{Pr}}{\pi(r_o^2 - r_i^2)} \int_{r_i}^{r_o} \int_0^{2\pi} \left(\frac{\partial\Theta}{\partial z}\right)_{z=1} s \, d\phi \, ds.$$

The linear analysis predicts that the primary bifurcation is in the form of a steadily retrogradely traveling wave concentrating in the outer sidewall region. This prediction is based on the most unstable linear mode which is described by Ra$_o = 34\,406$ with $m_o = 8$ and $\omega_o = 4.104$ for Ta$= 10^6$ and Pr$= 7.0$. Guided by the results of linear analysis, our numerical simulation begins at Ra$= 34\,000$, which is slightly below threshold, with an initial perturbation marked by the azimuthal wave number $m = 8$. Both E_{kin} and (Nu-1) decay towards zero after about 50 viscous diffusion times. At Ra $= 34\,600$, which is slightly above the onset of convective instabilities, a nonlinear equilibrium is reached after about 50 viscous diffusion times and is characterized by a steadily retrogradely traveling wave with frequency $\omega = 4.131$ and
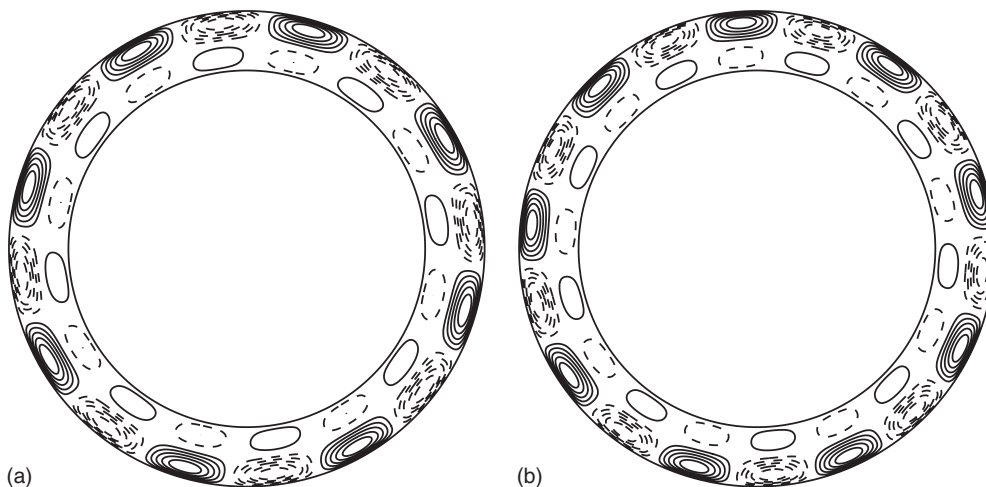
FIG. 6. Two nonlinear solutions in the form of a steadily retrogradely traveling wave obtained for $r_i = 1.5$ and $r_o = 2.0$: contours of u_z at the $z = 1/2$ horizontal plane for (a) Ra$= 34\,600$ and (b) Ra $= 34\,800$.

(a)

(b)
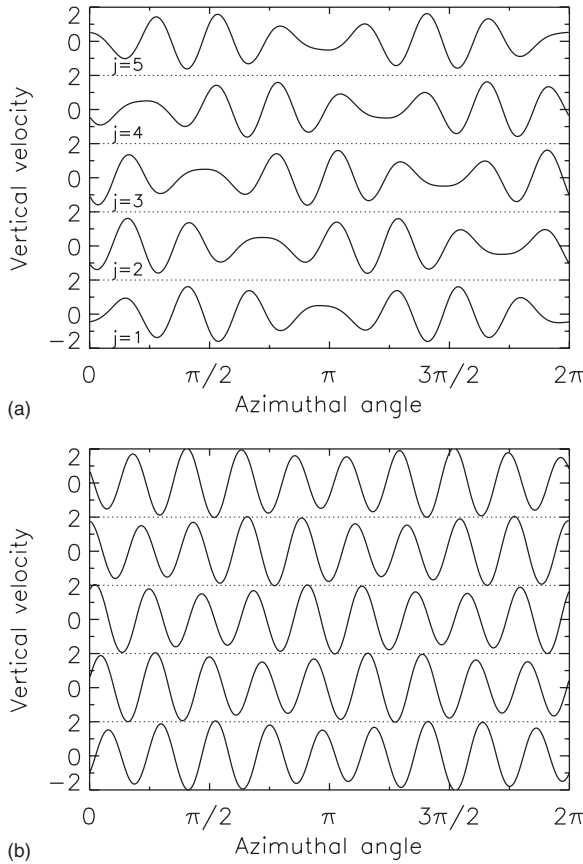
FIG. 7. A time-dependent nonlinear solution for $r_i=1.5$ and $r_o=2.0$ at Ra$=38\,000$: (a) $u_z(s=r_i+0.1)$ and (b) $u_z(s=r_o-0.1)$ at $z=1/2$ as function of ϕ plotted at five equally spaced instants $t=t_0+(j-1)0.2$, $j=1,2,\ldots,5$.

dominated by the azimuthal wave number $m=8$, indicating the bifurcation is supercritical. Both the kinetic energy E_{kin} and the Nusselt number Nu at Ra$=34\,600$ are time independent: $E_{kin}=0.1553$ and Nu$=1.019$. The spatial structure of the weakly nonlinear solution for Ra$=34\,600$ in a drifting frame is depicted in Fig. 6(a), showing a similar pattern to that obtained from the linear analysis.
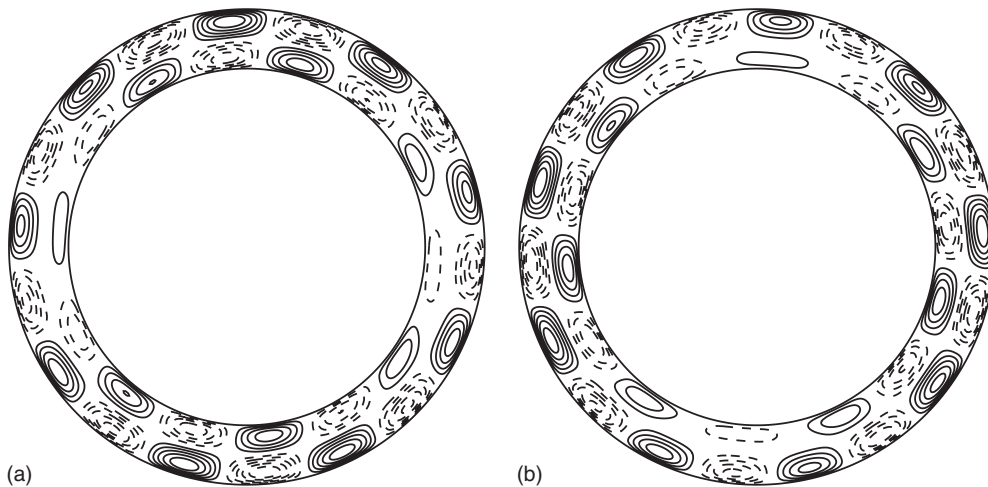
In addition to the steady retrograde wave with $m_o=8$, the convective excitation of the retrograde mode with $m_o=9$, whose onset is described by Ra$_o=34\,498$ with $\omega_o=3.957$, requires only a slightly higher Rayleigh number. We also carry out nonlinear simulations at Ra$=34\,800$ with the $m=9$ initial perturbation for Ta$=10^6$ and Pr$=7.0$ at the same radius ratio. In this case, the resulting nonlinear equilibrium is also in the form of a steadily retrogradely traveling wave but with dominant wave number $m=9$ and frequency $\omega=3.967$, the structure of which is depicted in Fig. 6(b). This has a constant kinetic energy $E_{kin}=0.1935$ and a constant Nusselt number Nu$=1.024$. In summary, when the Rayleigh number Ra is sufficiently near threshold, the bifurcation is supercritical and the inner prograde mode cannot be convectively excited.

C. Instabilities of the Eckhaus-Benjamin-Feir type: Modulated countertraveling waves

To illustrate the special feature of the secondary bifurcation via an instability of the Eckhaus-Benjamin-Feir type, it is desirable to look at the classical Eckhaus-Benjamin-Feir instability (e.g., Refs. [22,11]) in the context of a plane traveling wave whose amplitude A is described by the complex Ginzburg-Landau equation

$$A_t = \mu A + (1+i\gamma_1)A_{xx} - (1-i\gamma_2)|A|^2 A, \qquad (31)$$

where γ_1 and γ_2 are real and related to the effects of linear and nonlinear dispersion. When $\mu>0$, the trivial state loses stability to traveling wave solutions of the form

$$A = (\mu - m^2)\exp[i(mx-\omega t)], \qquad (32)$$

with $\omega=(\gamma_1 m^2+\gamma_2|A|^2)$, where $m=m_c+k$ with m_c being selected at onset. The steadily traveling wave solution (32) is similar to the primary bifurcation in the present problem. The Eckhaus-Benjamin-Feir instability describes how the traveling wave solution (32) becomes unstable, through a loss of energy from the most unstable wave number to nearby side bands, by resonant excitation of two neighboring waves with two wave numbers m_1 and m_2 satisfying $m_1+m_2=2m$ and

(a)   (b)

FIG. 8. Patterns of long wavelength modulated convection for $r_i=1.5$ and $r_o=2.0$ at Ra$=38\,000$: contours of u_z at the $z=1/2$ horizonal plane for two different instants.
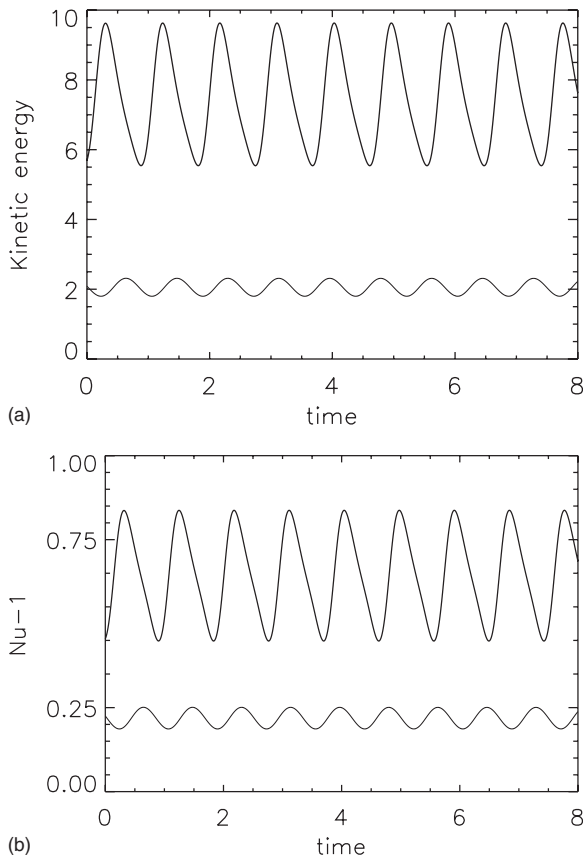
FIG. 9. Two nonlinear solutions for $r_i=1.5$ and $r_o=2.0$: (a) kinetic energies E_{kin} and (b) (Nu−1) as a function of time for two different Rayleigh numbers Ra=40 000 and 50 000 (from bottom up).

two frequencies satisfying $\omega_1+\omega_2=2\omega$. The instability usually leads to long wavelength modulations in the primary convection.

An interesting question in the present problem is the nature of the nonlinear instability of the steady retrograde wave and the resulting convection led by the instability when Ra

increases further. Our results suggest that the second bifurcation is, in some ways, connected with an Eckhaus-Benjamin-Feir instability. Figures 7 and 8 illuminate the key feature of the secondary nonlinear solution obtained at the Rayleigh number Ra=38 000. Figure 7(a) shows the vertical flow u_z evaluated at $z=1/2$ and $s=r_i+0.1$ as a function of the azimuthal angle ϕ at five different instants while Fig. 7(b) shows u_z at $z=1/2$ and $s=r_o-0.1$ as a function of ϕ at the same five different instants. The corresponding spatial patterns of nonlinear convection at two different instants are depicted in Fig. 8. It clearly demonstrates that the inner prograde mode marked by $Ra_i=35\,667$ with $m_i=7$ and $\omega_i=-4.053$, becomes convectively excitable at Ra=38 000. Consequently, the $m_1=7$ prograde mode interacting with a long wavelength mode $m_2=2$ results in spatial resonant excitation with the primary mode $m=9$ and in the long wavelength modulation shown in Fig. 8. In this sense, the second bifurcation is consistent with an Eckhaus-Benjamin-Feir instability in which a traveling wave becomes unstable to sideband modulations.

However, the instability mechanism in the present problem is quite different from that in the classical Eckhaus-Benjamin-Feir instability because (i) the neighboring traveling wave with $m=7$ is spatially located in the inner sidewall region while the primary mode concentrates in the outer sidewall region; (ii) the energy of the nonlinear instability is not from the most unstable wave number of the primary mode; and (iii) the resulting long wavelength modulation produces a unique convective flow that is temporally time-dependent and spatially nonperiodic but with a constant kinetic energy and Nusselt number, which are $E_{kin}=1.422$ and Nu=1.160 for Ra=38 000. The spatially nonperiodic pattern, shown in Figs. 7 and 8, varies constantly, depending upon the relative phase between the inner and outer traveling waves. Those differences are also indicative of the fact that the secondary convection solutions shown in Figs. 7 and 8 cannot be described by the complex Ginzburg-Landau equation (31).
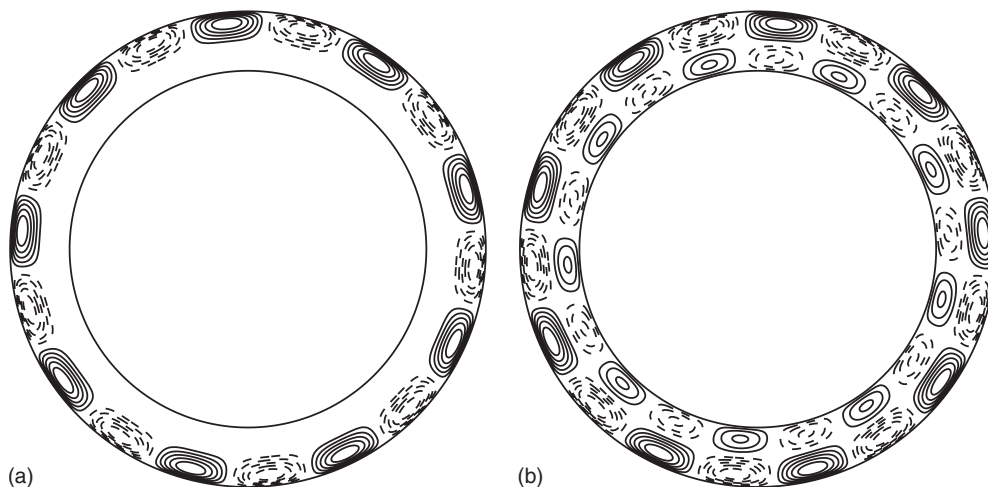
FIG. 10. The pattern of nonlinear convection for $r_i=1.5$ and $r_o=2.0$ obtained for Ra=40 000 at two different instants: (a) at an instant when E_{kin} and Nu reach a minimum while (b) shows an instant when E_{kin} and Nu reach a maximum.
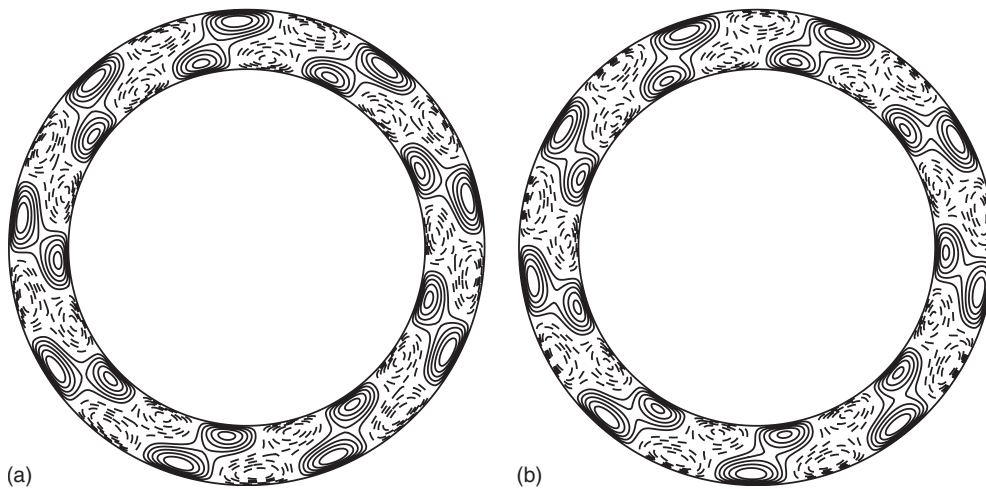
FIG. 11. Nonlinear convection in the form of the two-layered steadily retrogradely traveling wave for $r_i=1.5$ and $r_o=2.0$: contours of u_z in the $z=1/2$ horizontal plane for (a) Ra=67 500 and (b) Ra=70 000 in a drifting frame.

D. Destructive countertraveling waves

A remarkable and surprising nonlinear phenomenon occurs when the long-wavelength modulated convection becomes unstable, leading to destructive nonlinear interactions between the two countertraveling waves. When the Rayleigh number increases to Ra=40 000, the kinetic energy of convection becomes periodically time dependent, as is shown in Fig. 9, and the resulting convective flow vacillates between two different states: the single retrograde wave located in the outer sidewall region and the two countertraveling waves. The existence or disappearance of the prograde wave, which is spatially located in the inner sidewall region, is determined by its phase relative to the outer retrograde wave. The convection patterns of the two different states obtained at two different instants are displayed Fig. 10.

It is the switch of the azimuthal wave number, from m =7 to 9, of the inner prograde wave that characterizes the nonlinear instability and causes the spatially resonant or destructive interaction between the inner prograde wave and the outer retrograde wave. The linear analysis predicts that the inner prograde wave with $m_i=9$ and $\omega_i=-3.749$ can be convectively excited for $Ra>Ra_i=37\,482$. When Ra $\geqslant 40\,000$, the secondary bifurcation marked by the $m_i=7$ inner prograde wave becomes unstable to the $m_i=9$ prograde wave, hence leading to destructive nonlinear interaction between the two countertraveling waves with exactly the same wave number. At an instant when the phase of the inner prograde wave is the same as that of the outer retrograde wave, the prograde wave is destroyed and disappears, as shown in Fig. 10(a). The corresponding kinetic energy E_{kin} and the Nusselt number Nu reach a minimum with E_{kin} =1.800 and the Nusselt number Nu−1=0.1866. When the inner prograde wave is out of phase with the outer retrograde wave, the prograde wave survives and the corresponding E_{kin} and Nu reach a maximum with E_{kin}=2.312 and Nusselt number (Nu−1)=0.2506. For larger values of the Rayleigh number, for example, at Ra=50 000 which is also shown in Fig. 9, the inner prograde wave can survive but is weak when the two countertraveling waves are in the same phase.

E. Saddle-node-type bifurcation

It is anticipated that, when Ra increases further, the inner prograde wave becomes increasingly more competitive and

cannot be eradicated by its nonlinear resonant interaction with the outer retrograde wave. For sufficiently large values of Ra, for example, at Ra=55 000, it is found that the convective flow consists of two countertraveling waves that have the same wave number $m=9$, coexisting and interacting nonlinearly. But the inner prograde wave is always slightly weaker than the outer retrograde wave and, consequently, is always under the influence of the outer retrograde wave.

The physical situation is, in some aspects, analogous to the nonlinear convection in spherical rotating systems sub-
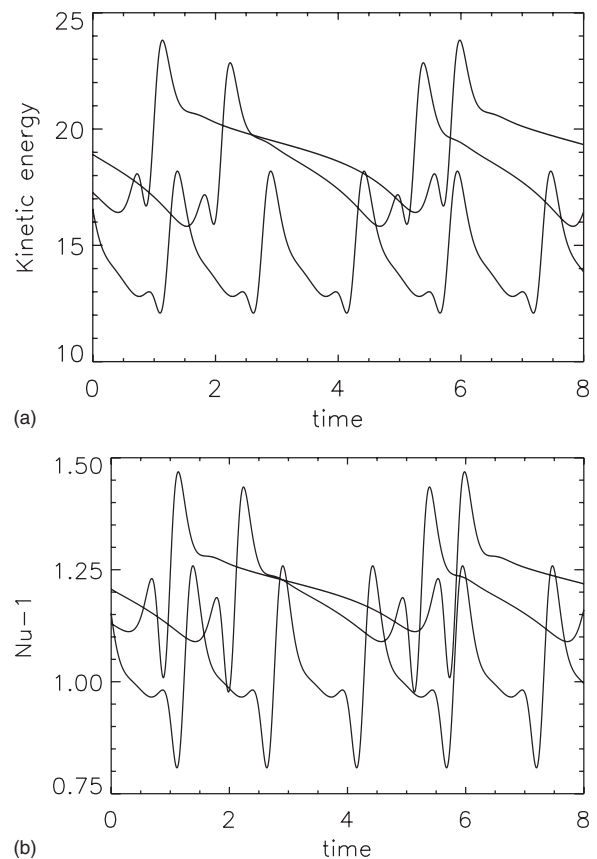
FIG. 12. Three nonlinear solutions for $r_i=1.5$ and $r_o=2.0$: (a) kinetic energies E_{kin} and (b) (Nu−1) as a function of time for three different Rayleigh numbers with Ra=60 000, 65 000, 66 000 (from bottom up).
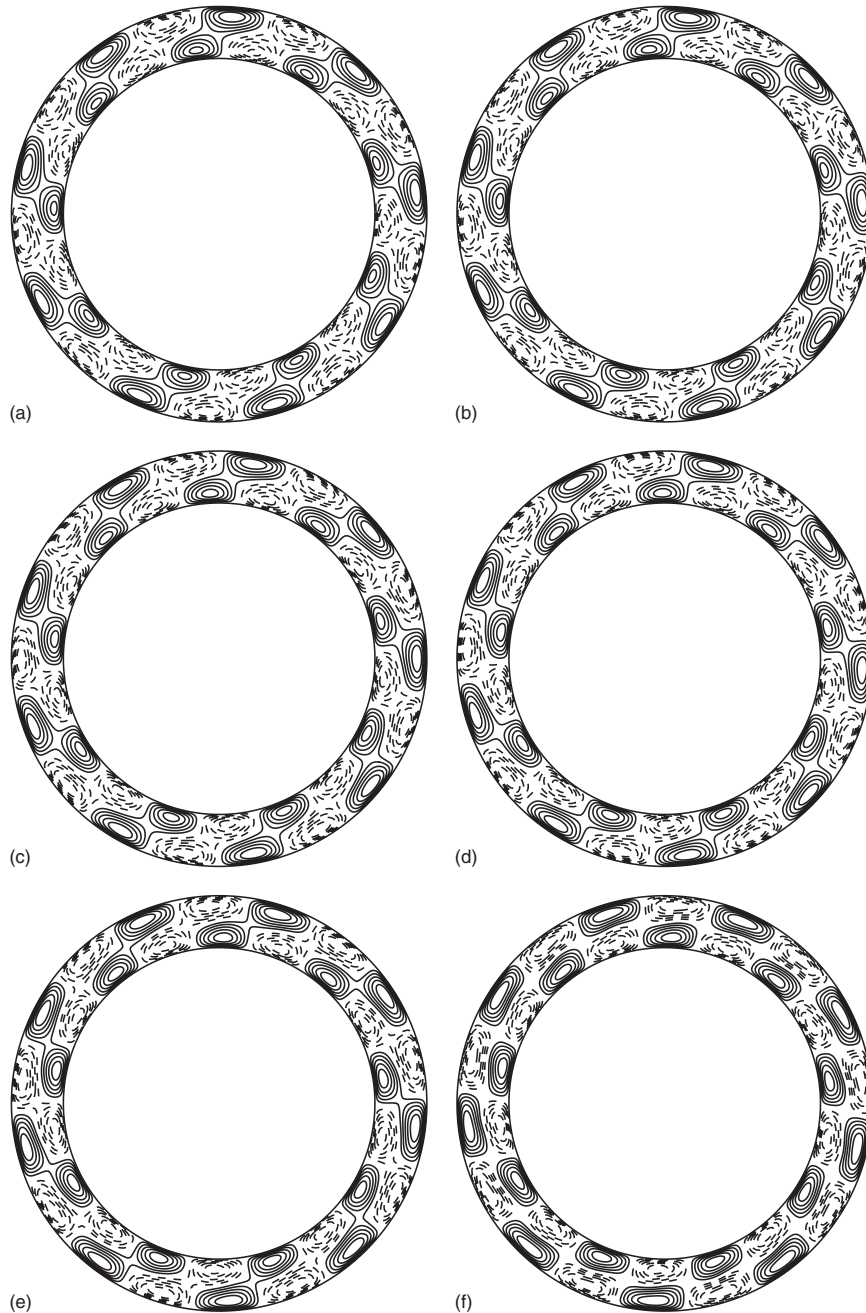
FIG. 13. The time-dependent patterns of nonlinear convection for $r_i=1.5$ and $r_o=2.0$ at Ra=65 000, showing contours of u_z at the $z=1/2$ horizonal plane at six equally spaced instants during a period of the oscillation.

ject to a spatially nonuniformly heated outer surface [24], a phenomenon in the context of understanding the correlation between the main features of the geomagnetic field at the core-mantle boundary and the temperature anomalies in the lower mantle. It was found that, when the convection modes and the boundary anomalies have the same wavelength and hence are spatially resonant, the traveling wave convection locks to the boundary anomalies giving configurations that are stable for long periods of time, interspersed by intervals of rapid change. In the present problem, if the outer retrograde wave is treated as the nonuniform boundary condition for the inner prograde wave, the two problems are dynamically similar.

Prior to discussing the nonlinear phenomenon involved in the two countertraveling waves, it is profitable to look at the basic idea of the saddle-node bifurcation. This is a local bifurcation in which two fixed points or two equilibrium states of a dynamical system collide and annihilate each other at a particular value of the control parameter: one of the equilibrium states is unstable (the saddle) while the other is stable (the node). In the vicinity of the saddle-node point, the dynamical system varies slowly and takes a nearly infinitely long time to depart from the unstable equilibrium state.

For the purpose of understanding our rotating convection, we look at the nonlinear behavior by letting Ra gradually decrease from a sufficiently large value at which the outer

retrograde wave becomes strong enough to lock the weaker inner prograde wave. In other words, the nonlinear convection is in the form of a two-layered steadily retrogradely traveling wave, representing one stable equilibrium state for larger Rayleigh numbers. Two such nonlinear convection solutions obtained for Ra=67 500 and Ra=70 000 are shown in Fig. 11 in a drifting frame. It is of importance to note that the whole pattern in Fig. 11, i.e., both the inner and outer layers, moves together retrogradely. For smaller values of Ra, say at Ra=60 000, there exists a different nonlinear equilibrium representing the two coexisting, nonlinearly interactive countertraveling waves. Between the two different equilibria, there exists a saddle-node point (the coalescence and disappearance of the two nonlinear equilibria) marked by a particular Rayleigh number Ra_s which is about 67 000 for Ta $=10^6$ and Pr=7.0. Slightly below the saddle-node point, the two-layered retrograde wave in Fig. 11 becomes unstable, leading to an oscillatory convection. The period of oscillation is numerically very long and mathematically approaching infinity in the limit Ra$\rightarrow$Ra$_s$. An example of this nonlinear behavior is illustrated in Fig. 12 where three nonlinear solutions obtained for three different Rayleigh numbers Ra $=60 000, 65 000, 66 000$, are displayed, showing that the oscillation period increases from 1.5 at Ra=60 000 to 5.1 at Ra=66 000 as Ra approaches the saddle-node point.

Physically speaking, the behavior of the nonlinear convection is clear: the stronger retrograde wave tends to lock the inner prograde wave that attempts to move progradely away from the outer retrograde wave. This physics is perhaps most clearly illuminated in the evolution of the convection patterns displayed in Fig. 13 for six equally spaced instants. The propagation of the inner prograde wave nearly stops when there is moderate phase difference between the two waves. But the inner wave moves quickly when it is out of phase with the outer retrograde wave. Mathematically speaking, this corresponds to a saddle-node-type bifurcation: two distinct nonlinear equilibria—the two-layered steady retrograde wave and the two countertraveling waves—collide and disappear at a particular value of the Rayleigh number, leaving a new slowly time-dependent convection solution. Although this is a quite common nonlinear phenomenon in simple dynamical systems governed by an ordinary differential equation, to the authors' knowledge, this is the first time that a saddle-node-type bifurcation has been found in a rotating convection system that has homogeneous boundary conditions and is governed by partial differential equations.

V. CONCLUDING REMARKS

We have investigated both linear and nonlinear convection in a fluid-filled annular cylinder, with realistic no-slip boundary conditions, uniformly heated from below and rotating about a vertical axis. The linear stability analysis reveals the existence of two counter-traveling waves—retrogradely propagating waves near the outer sidewall and progradely propagating waves adjacent to the inner sidewall—which is central to understanding the properties of
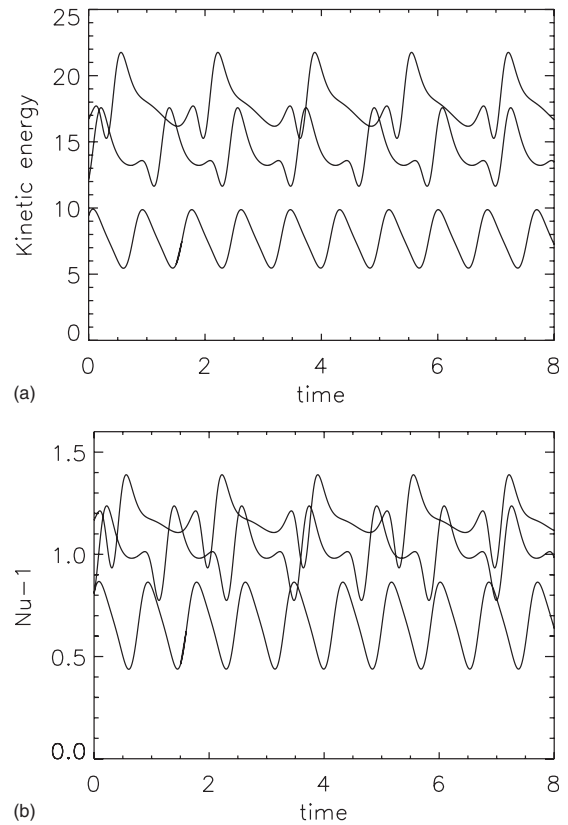
FIG. 14. Three nonlinear solutions for $\chi=0.75$ and $r_o=2.0$ at Pr=7.0 (a) kinetic energies E_{kin} and (b) (Nu−1) as a function of time for three different Rayleigh numbers: Ra $=50 000, 60 000, 65 000$ (from bottom up).

nonlinear convection. As a result of the cylindrical curvature, the two counter-traveling modes have different wave numbers, frequencies and critical Rayleigh numbers. Of a large number of the numerical simulations carried out, only several representative solutions are presented. The nonlinear simulations reveal three interesting new nonlinear solutions in rotating Rayleigh-Bénard convection: tempospatially modulated countertraveling waves caused by an instability of the Eckhaus-Benjamin-Feir type, destructive countertraveling waves and a saddle-note-type bifurcation. Since the nonlinear convection solutions are obtained for fluid-filled annular cylinders with Pr=7.0 with a moderate rate of rotation under experimental boundary conditions, these nonlinear phenomena should be readily observable in laboratory experiments.

Finally, we would like to mention the possible multiplicity of nonlinear equilibria. It is common in nonlinear convection that several different solutions can exist and are stable at exactly the same Rayleigh number Ra. In the present problem, since there exist a number of the neighboring linear modes such as $m_o=8$ and 9 that have slightly different values of Ra, it is not surprising that multiple nonlinear solutions can exist and are stable. By using different initial perturbations in our numerical simulation, we are able to obtain different nonlinear solutions at exactly the same parameters. For example, with an $m=8$ initial perturbation, we

have also simulated nonlinear convection for Ra $=50\,000,60\,000,65\,000$ at Pr$=7.0$ and Ta$=10^6$, as are depicted in Fig. 14. Except for changing the dominant wave number from $m=9$ to 8, the nonlinear solutions in Fig. 14 exhibit similar features to those illustrated in Fig. 12. Of course, our numerical approach cannot provide the general mathematical picture of multiple nonlinear solutions in the present problem.

[1] F. Zhong, R. E. Ecke, and V. Steinberg, Phys. Rev. Lett. **67**, 2473 (1991).

[2] J. Herrmann and F. H. Busse, J. Fluid Mech. **255**, 183 (1993).

[3] Y. Liu and R. E. Ecke, Phys. Rev. Lett. **78**, 4391 (1997).

[4] E. Plaut and F. H. Busse, J. Fluid Mech. **464**, 345 (2002).

[5] J. M. Aurnou, S. Andreadis, L. Zhu, and P. L. Olson, Earth Planet. Sci. Lett. **212**, 119 (2003).

[6] J. Rotvig and C. A. Jones, J. Fluid Mech. **567**, 117 (2006).

[7] K. Zhang and X. Liao, J. Fluid Mech. **610**, 425 (2008).

[8] H. F. Goldstein, E. Knobloch, I. Mercader, and M. Net, J. Fluid Mech. **248**, 583 (1993).

[9] E. Y. Kuo and M. C. Cross, Phys. Rev. E **47**, R2245 (1993).

[10] K. Zhang, X. Liao, and F. H. Busse, J. Fluid Mech. **578**, 371 (2007).

[11] E. Knobloch, in *Lectures on Solar and Planetary Dynamos*, edited by M. R. E. Proctor and A. D. Gilbert (Cambridge University Press, Cambridge, 1993), pp.331–372.

[12] E. Knobloch, Phys. Fluids **8**, 1446 (1996).

[13] J. M. Aurnou, M. Heimpel, L. Allen, E. King, and J. Wicht, Geophys. J. Int. **173**, 793 (2008).

[14] M. van Hecke and W. van Saarloos, Phys. Rev. E **55**, R1259 (1997).

[15] E. Serre, E. C. del Arco, and F. H. Busse, in *Nonlinear Dynamics in Fluids*, edited by F. Marqués and A. Meseguer (CIMNE, Barcelona, 2003), pp. 138–140.

[16] E. Plaut, Phys. Rev. E **67**, 046303 (2003).

[17] L. Li, X. Liao, and K. Zhang, Phys. Rev. E **77**, 027301 (2008).

[18] X. Liao, K. Zhang, and Y. Chang, J. Fluid Mech. **549**, 375 (2006).

[19] F. Marqués, Phys. Fluids A **2**, 729 (1990).

[20] F. H. Harlow and J. E. Welch, Phys. Fluids **8**, 2182 (1965).

[21] J. K. Dukowicz and A. S. Dvinsky, J. Comput. Phys. **102**, 336 (1992).

[22] T. Benjamin and J. Feir, J. Fluid Mech. **27**, 417 (1967).

[23] A. M. Soward, Geophys. Astrophys. Fluid Dyn. **9**, 19 (1977).

[24] K. Zhang and D. Gubbins, J. Fluid Mech. **250**, 209 (1993).